

# Origin of the high-energy Raman modes in single-wall carbon nanotubes

J. Maultzsch, C. Thomsen, S. Reich, and M. Machón

*Institut für Festkörperphysik, Hardenbergstr. 36, 10623 Berlin, Germany*

**Abstract.** We present a new interpretation of the origin of the first-order Raman modes in single-wall carbon nanotubes. Similar to the disorder-induced  $D$  mode, the high-energy modes are determined by double-resonant scattering. Our model predicts an excitation-energy dependence of the Raman frequencies, which we observe experimentally as well. We present preliminary results on the Raman spectra of metallic tubes.

The origin of the first-order high-energy Raman modes in carbon nanotubes has been a puzzling question since the first Raman measurements on single-wall tubes by Rao *et al.* [1]. The high-energy Raman spectrum (often called  $G$  band) exhibits two prominent peaks, a larger one at  $\approx 1590 \text{ cm}^{-1}$  above and a smaller one at  $\approx 1570 \text{ cm}^{-1}$  below the graphite  $\Gamma$ -point frequency; additional smaller structures appear towards lower frequencies. Some authors suggested that they originate from different phonon bands folded into the  $\Gamma$  point, which have  $A_{1(g)}$ ,  $E_{1(g)}$ , and  $E_{2(g)}$  symmetry (the subscript  $g$  refers to achiral tubes). Contrary to this interpretation, it was shown experimentally, that the complete high-energy peak structure corresponds mainly to the fully symmetric  $A_{1(g)}$  phonon modes [2, 3, 4]. All attempts to explain the origin of the high-energy modes that have been made so far, implicitly assume that they correspond to  $\Gamma$ -point phonons.

Here we show that a defect-induced, double resonant Raman process [5] naturally leads to the observed high-energy spectrum with only  $A_{1(g)}$  phonons involved. These phonons stem from a region inside the Brillouin zone near the  $\Gamma$  point; their wave vectors are – in contrast to usual first-order scattering – considerably larger (up to a factor of 100) than the wave vector of the incoming light. Defect-induced, double resonant Raman scattering has been well established to lead to the  $D$  mode ( $\approx 1350 \text{ cm}^{-1}$ ) in the first-order Raman spectrum of graphite and carbon nanotubes [5, 6, 7]. The  $D$  mode exhibits the characteristic feature of a double-resonant Raman process, that is the excitation-energy dependence of the Raman frequency. The scattering process for the  $D$  mode involves only phonons which, in the zone-folding picture, scatter the electron between two inequivalent  $K$  points of the graphene Brillouin zone. Another possible double-resonant process is the scattering across the minimum at the  $K$  point, which has been recently investigated by Saito *et al.* for graphite [8]. Such phonons possess wave vectors  $q$  up to  $q \approx 0.2\pi/a_0$  ( $a_0$  is the graphene lattice constant), which is small compared with the wave vectors of the  $D$ -mode phonons. They lead to Raman frequencies close to the  $\Gamma$ -point frequencies. In chiral tubes, there are two optical phonon branches with  $A_1$  symmetry at the  $\Gamma$  point which give rise to two peaks in the Raman spectrum. In Fig. 1 we show a scattering process with an incoming resonance (solid arrow) and resonant

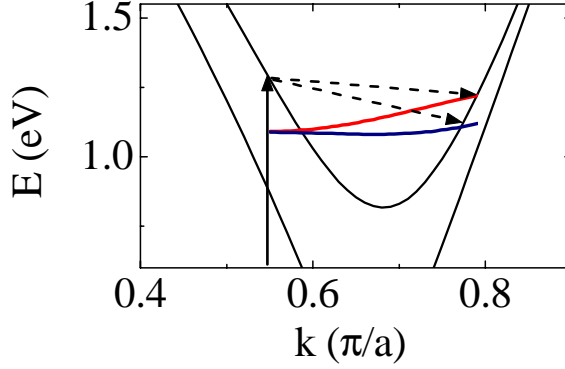


**FIGURE 1.** Double resonant scattering process leading to the high-energy modes. The solid arrow indicates an resonant absorption of a photon. The near  $\Gamma$ -point part of the phonon dispersion is shown schematically, at the intersection with the electronic bands the excited electron is scattered in another resonant transition (dashed arrows).

scattering of the excited electron by a phonon (dashed arrow). The angular momentum quantum number of  $A_{1(g)}$  phonons is  $\tilde{m} = 0$ ; therefore the electron is always scattered within the same band by the phonon. In the zone-folding picture, the  $\tilde{m} = 0$  phonon branches contain the  $\Gamma$  point of graphite. The two  $\tilde{m} = 0$  optical branches near the  $\Gamma$  point are depicted schematically with the  $\Gamma$  point at the wave vector of the excited electron; the phonon energy axis is inverted to indicate Stokes scattering. Out of all transitions the resonantly excited electron can make, the intersection points of the phonon and electron dispersion indicate the resonant ones. The phonon wave vector and frequency for such a resonant transition are uniquely determined for each phonon branch; the Raman signal at this frequency is strongly enhanced.

As a first approximation, we used a model phonon dispersion relation based on the dispersion of graphene. The upper branch exhibits an overbending, i.e., the maximum phonon frequency occurs away from the  $\Gamma$  point. The magnitude of a (possible) splitting of the  $\Gamma$ -point phonons does not influence the general results or the consequences of our model, because the involved phonon wave vectors are sufficiently large. For simplicity, we took the electronic band structure in the symmetry-based tight-binding approximation [9]. We calculated the Raman cross section as a function of the phonon energy according to a second-order process with a defect involved in one of the transitions [6]. The matrix elements were assumed to be wave-vector independent, but we included them in terms of selection rules for electron-photon and electron-phonon coupling.

In Fig. 2 (*left*) we show a calculated Raman spectrum of the (15,6) tube (lower curve) for an excitation energy 2.18 eV. The upper curve is an experimental spectrum of bundled single-wall nanotubes with a mean tube diameter of 1.45 nm taken at the same energy. The experimental spectrum is very well reproduced by our calculation. There

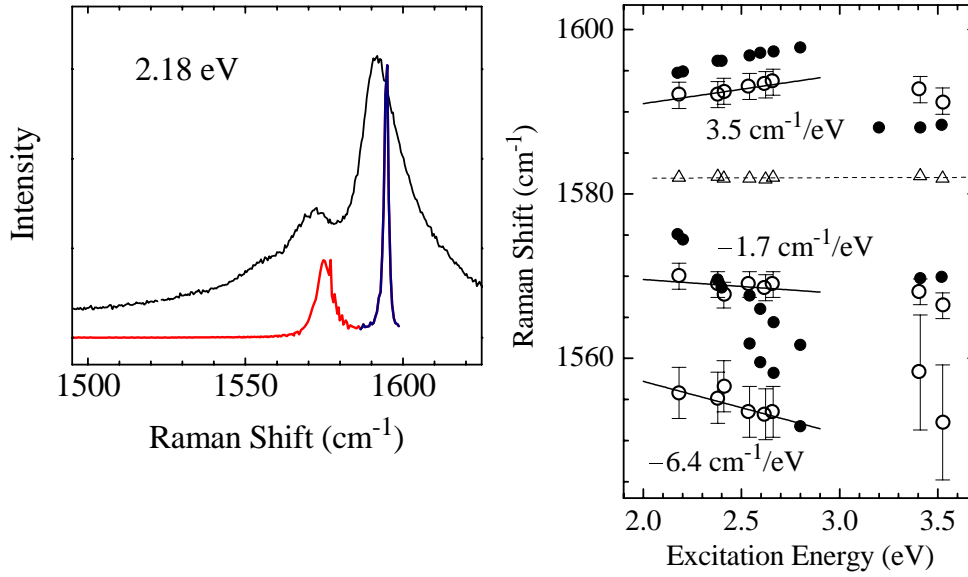


**FIGURE 2.** *Left:* Calculated Raman spectra for the (15,6) tube (lower curve) for an excitation energy 2.18 eV, and experimental Raman spectrum (upper curve) of tubes with diameter 1.4 nm at the same excitation energy. *Right:* Experimental (open circles) and theoretical (closed circles) values for the frequencies of the high-energy Raman modes. Triangles indicate the position of the graphite G mode.

is a minimum between the two largest peaks around the graphite  $\Gamma$ -point frequency ( $1588 \text{ cm}^{-1}$  in our model dispersion); the upper peak has a larger amplitude than the lower one. The model comprises the smaller structures in the high-energy range as well. At a given laser energy, several electronic bands can be involved, which leads to a signal from phonons of the same branch with different wave vectors and hence frequency. In principle, those processes contribute more to the Raman signal which occur at a higher electronic density of states (smaller phonon wave vectors). Therefore, depending on the particular tube and the laser energy, contributions from other electronic bands vary in intensity compared to the strongest peaks. For the same reason, the absolute intensities depend on the laser energy as well; for tubes with diameters between 1.3 nm and 1.5 nm and excitation energies in the range of visible light, the Raman intensity decreases with increasing laser energy. Finally, we find an excitation-energy dependence of the Raman frequencies both in experiment and theory [10] which is the signature of a double-resonant process. In Fig. 2 (*right*) the experimental and theoretical frequencies of the high-energy modes are shown by open and closed circles, respectively, as a function of excitation energy. The upper peak shifts towards higher frequency, which reflects the overbending in the upper phonon branch, while the frequency of the lower peak decreases with increasing laser energy. For comparison, the Raman frequency of graphite is indicated (triangles), which does not depend on the laser energy.

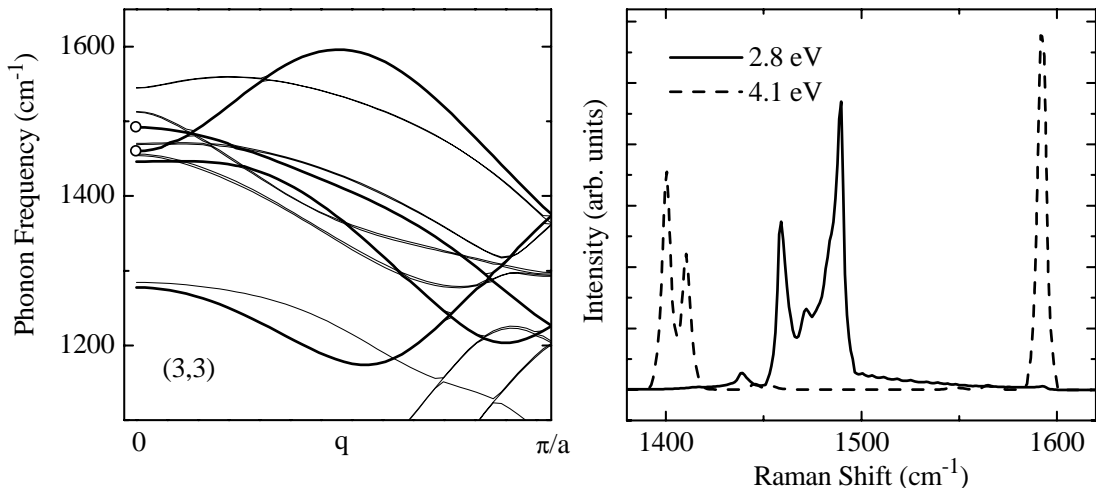


**FIGURE 3.** (Left:) Phonon dispersion relations of the (3,3) tube from *ab initio* calculations within the local-density function approximation. Thick lines:  $\tilde{m} = 0$  branches; circles:  $\Gamma$ -point frequencies of the LO and TO-like phonons. (Right:) Calculated Raman spectra of the (3,3) tube for an excitation energy 2.8 eV (solid line) and 4.1 eV (dashed line).

The Raman spectra shown in Fig. 2 with two prominent peaks at  $\approx 1570$  and  $\approx 1590$   $\text{cm}^{-1}$  are often called “semiconducting” spectra. They typically appear at laser energies around the transition energies between the singularities in the electronic density of states for *semiconducting* tubes. Note that our calculation for the metallic (15,6) tube also yields a “semiconducting” spectrum. On the other hand, typical spectra from bulk samples which are attributed to metallic tubes exhibit a broad structure in the range from 1500 to 1600  $\text{cm}^{-1}$ , centered at lower frequency than the “semiconducting” spectra. This broadening and downshift of the high-energy peaks has been attributed to a coupling between the phonons and the conduction electrons in metallic tubes, resulting in a Fano-lineshape [11, 12]. The experimental peak shape and frequencies, however, have not been reproduced by calculations so far, and the question arises whether also these “metallic” spectra can be explained within the double-resonance model.

The phonon dispersion of metallic tubes at the  $\Gamma$  point is probably not sufficiently well described by our simple model dispersion based on graphene. In Fig. 3 (left) we show the phonon dispersion of the (3,3) tube from an *ab initio* calculation [13] within the local-density function approximation [14]. The  $\Gamma$ -point frequencies of the  $\tilde{m} = 0$  branches (circles) are at 1470  $\text{cm}^{-1}$  and 1490  $\text{cm}^{-1}$ , which is by about 100  $\text{cm}^{-1}$  lower than the graphite  $\Gamma$ -point frequency. This agrees well with the work by Kresse *et al.*, who in a similar *ab initio* calculation for larger armchair and zig-zag tubes found a decrease of the  $\Gamma$ -point frequencies in metallic tubes by some tens of wave numbers compared with those of semiconducting tubes [15].

On the other hand, one of these phonon branches exhibits a strong overbending up to  $\approx 1600$   $\text{cm}^{-1}$  inside the Brillouin zone. In armchair tubes, phonons from this branch are actually forbidden by symmetry in a Raman process. But we expect a similar dispersion in chiral metallic tubes and therefore use this armchair dispersion as an example. If in a double-resonant Raman process the singularity in the electronic

joint density of states is nearly matched, the phonon wave vectors are very small and frequencies almost at the  $\Gamma$ -point frequencies are observed. We therefore suggest that this is the origin of the large downshift in the “metallic” spectra. In Fig. 3 (*right*) we show some preliminary calculations of the Raman spectra of a (3,3) tube. For the electron band structure we used an *ab initio* calculation as well; the first singularity appears around 2.8 eV [16]. Therefore the spectrum with the laser energy at 2.8 eV (solid line) shows approximately the  $\Gamma$ -point phonon frequencies. If the laser energy is increased and hence the wave vectors of the involved phonons become larger, the observed Raman frequencies increase up to the maximum frequency around  $1600\text{ cm}^{-1}$ . This is shown for a laser energy of 4.1 eV (dashed line), where again a narrow peak at  $1600\text{ cm}^{-1}$  appears.

In conclusion, we showed that the high-energy Raman process in single-wall carbon nanotubes is the same as for the disorder-induced *D* mode. We have reproduced the high-energy spectrum by our calculations of a defect-induced, double-resonant Raman process. Our model is supported by the dependence of the high-energy Raman frequencies on excitation-energy. Finally, we showed that Raman spectra usually attributed to semiconducting tubes can also originate from metallic tubes, while “metallic” spectra probably stem from metallic tubes exclusively.

## REFERENCES

1. Rao, A. M., Richter, E., Bandow, S., Chase, B., Eklund, P. C., Williams, K. A., Fang, S., Subbaswamy, K. R., Menon, M., Thess, A., Smalley, R. E., Dresselhaus, G., and Dresselhaus, M. S., *Science*, **275**, 187 (1997).
2. Duesberg, G. S., Loa, I., Burghard, M., Syassen, K., and Roth, S., *Phys. Rev. Lett.*, **85**, 5436 (2000).
3. Jorio, A., Dresselhaus, G., Dresselhaus, M. S., Souza, M., Dantas, M. S. S., Pimenta, M. A., Rao, A. M., Saito, R., Liu, C., and Cheng, H. M., *Phys. Rev. Lett.*, **85**, 2617 (2000).
4. Reich, S., Thomsen, C., Duesberg, G. S., and Roth, S., *Phys. Rev. B*, **63**, R041401 (2001).
5. Thomsen, C., and Reich, S., *Phys. Rev. Lett.*, **85**, 5214 (2000).
6. Maultzsch, J., Reich, S., and Thomsen, C., *Phys. Rev. B*, **64**, 121407(R) (2001).
7. Kürti, J., Zólyomi, V., Grüneis, A., and Kuzmany, H., *Phys. Rev. B* (2002, in print).
8. Saito, R., Jorio, A., Filho, A. G. S., Dresselhaus, G., Dresselhaus, M. S., and Pimenta, M. A., *Phys. Rev. Lett.*, **88**, 027401 (2002).
9. Damjanović, M., Vuković, T., and Milošević, I., *J. Phys. A: Math. Gen.*, **33**, 6561 (2000).
10. Maultzsch, J., Reich, S., and Thomsen, C., *Phys. Rev. B* (2002, in print).
11. Pimenta, M. A., Marucci, A., Empedocles, S. A., Bawendi, M. G., Hanlon, E. B., Rao, A. M., Eklund, P. C., Smalley, R. E., Dresselhaus, G., and Dresselhaus, M. S., *Phys. Rev. B*, **58**, R16 016 (1998).
12. Brown, S. D. M., Jorio, A., Corio, P., Dresselhaus, M. S., Dresselhaus, G., Saito, R., and Kneipp, K., *Phys. Rev. B*, **63**, 155414 (2001).
13. Sánchez-Portal, D., Ordejón, P., Artacho, E., and Soler, J. M., *Int. J. Quantum Chem.*, **65**, 453 (1997).
14. Machón, M., Reich, S., Thomsen, C., and Ordejón, P. (unpublished).
15. Kresse, G., and Dubay, O., “Phonon softening in metallic nanotubes through a Peierl’s mechanism,” in *Electronic Properties of Novel Materials-Molecular Nanostructures*, edited by H. Kuzmany, J. Fink, M. Mehring, and S. Roth, AIP, 2002, p. xxx.
16. Machón, M., Reich, S., Thomsen, C., Ordejón, P., and Sánchez-Portal, D. (2002, submitted to *Phys. Rev. B*).